The Journal of Chemical Physics ARTICLE scitation.org/journal/jcp

Excited-state resonance Raman spectroscopy probes the sequential two-photon excitation mechanism of a photochromic molecular switch

Cite as: J. Chem. Phys. 157, 234302 (2022); doi: 10.1063/5.0126974
Submitted: 18 September 2022 • Accepted: 22 November 2022 •
Published Online: 15 December 2022

Kristen H. Burns, Timothy J. Quincy,[a] and Christopher G. Elles[b]

AFFILIATIONS

Department of Chemistry, University of Kansas, Lawrence, Kansas 66045, USA

[a]**Current address:** Department of Science, Technology, and Mathematics, Lincoln University, Jefferson City, Missouri 65101, USA.
[b]**Author to whom correspondence should be addressed:** elles@ku.edu

ABSTRACT

Some diarylethene molecular switches have a low quantum yield for cycloreversion when excited by a single photon, but react more efficiently following sequential two-photon excitation. The increase in reaction efficiency depends on both the relative time delay and the wavelength of the second photon. This paper examines the wavelength-dependent mechanism for sequential excitation using excited-state resonance Raman spectroscopy to probe the ultrafast (sub-30 fs) dynamics on the upper electronic state following secondary excitation. The approach uses femtosecond stimulated Raman scattering (FSRS) to measure the time-gated, excited-state resonance Raman spectrum in resonance with two different excited-state absorption bands. The relative intensities of the Raman bands reveal the initial dynamics in the higher-lying states, S_n, by providing information on the relative gradients of the potential energy surfaces that are accessed via secondary excitation. The excited-state resonance Raman spectra reveal specific modes that become enhanced depending on the Raman excitation wavelength, 750 or 400 nm. Many of the modes that become enhanced in the 750 nm FSRS spectrum are assigned as vibrational motions localized on the central cyclohexadiene ring. Many of the modes that become enhanced in the 400 nm FSRS spectrum are assigned as motions along the conjugated backbone and peripheral phenyl rings. These observations are consistent with earlier measurements that showed higher efficiency following secondary excitation into the lower excited-state absorption band and illustrate a powerful new way to probe the ultrafast dynamics of higher-lying excited states immediately following sequential two-photon excitation.

I. INTRODUCTION

Photochromic compounds based on a central diarylethylene framework have found widespread use as thermally stable, optically reversible molecular switches.[1–8] Many such systems undergo reversible electrocyclization and cycloreversion reactions when exposed to UV and visible light, respectively.[9–12] For example, the compound in Fig. 1, which we label as DAE throughout this paper, is a prototypical diarylethylene-based molecular switch. DAE undergoes efficient ring-closure upon irradiation of the open-ring isomer with UV light, whereas excitation of the closed-ring isomer with visible light results in ring-opening with a quantum yield less than ~0.02.[13–18]

A low cycloreversion yield is favorable for applications that require read-out of the molecular state without converting the molecule back to the open-ring isomer, but an alternate means of reversion is necessary for maintaining switchability.[1,2,17,19] Along these lines, a series of insightful measurements by Miyasaka and co-workers[13,14,20,21] revealed a "gated" photoswitching mechanism in which the low cycloreversion yield of several photochromic molecules, including DAE, could be overcome by sequential excitation with two time-delayed photons. The initial studies noted that enhanced photoswitching was only observed for irradiation with intense ps-duration laser pulses, whereas excitation with fs-duration laser pulses of comparable intensity did not increase the reaction yield compared to one-photon excitation at low power.[13]

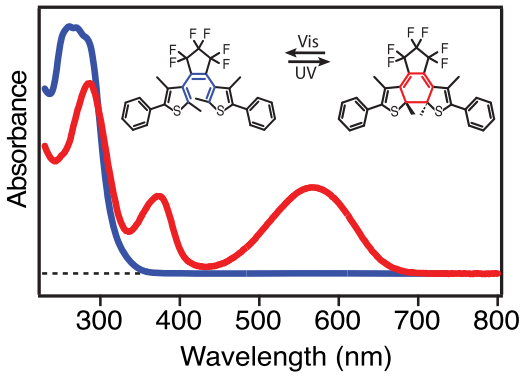

FIG. 1. Absorption spectra of the open- and closed-ring isomers of 1,2-bis(2,4-dimethyl-5-phenyl-3-thienyl)-perfluorocyclopentene, DAEo and DAEc, respectively.

Those authors proposed a mechanism in which the molecule must evolve in time between the initial excitation with one photon and re-excitation with a second photon from the same laser pulse.[13,20] Indeed, more recent measurements using independent time-delayed fs laser pulses by our group and others confirm that the sequential two-photon excitation mechanism requires evolution in the initially excited state before the absorption of a second photon accesses a higher-lying electronic state that more efficiently drives the cycloreversion reaction.[13–15,22–25] Furthermore, the sequential two-photon excitation mechanism for DAE depends on the wavelength of the second photon, which implies that accessing different higher-lying states induces different reaction dynamics.[16,23]

Previous ultrafast measurements probed the sequential excitation mechanism using transient absorption (TA) spectroscopy with a pump–repump–probe pulse sequence.[13,14,17,24,26,27] For example, a change in the ground-state bleach intensity at time delays that are much longer than the excited-state lifetime helps probe the impact of sequential two-photon excitation on the cycloreversion quantum yield compared to excitation by either of the individual photons on their own. Notably, we showed that the increase of the reaction yield depends on both the wavelength and the relative time delay of the secondary (re-pump) excitation pulse.[23] Similar measurements probing the evolution of the TA signal at very short time delays revealed the spectral signature of a short-lived (~200 fs) species immediately after secondary excitation, which we attributed to the fleeting population of a higher-lying electronically excited state.[23] The TA measurements provide only limited information about the dynamics following sequential excitation, due to the very short lifetimes and broad, overlapping electronic absorption bands. Therefore, the current study turns to excited-state resonance Raman spectroscopy as a means of probing the ultrafast dynamics in the higher-lying states following secondary excitation.

Analogous to traditional resonance Raman spectroscopy starting from the ground-state,[28–33] excited-state resonance Raman measurements provide information about the higher-lying states based on mode-specific enhancements of the vibrational scattering signal.[34–36] Briefly, the frequencies in a resonance Raman spectrum report on the structure of the lower electronic state, whereas mode-specific enhancements reflect the relative gradient (or displacement) of the upper-state potential energy surface along each of those vibrational coordinates. In other words, the relative Raman scattering intensities reveal the initial motions of the wave packet upon excitation by highlighting which modes are Franck–Condon (FC) active. In the case of excited-state resonance Raman measurements, the vibrational frequencies reflect the structure of the molecule in the first excited state, S_1, whereas the relative intensities provide information about the higher-lying electronic states, S_n.

The femtosecond stimulated Raman scattering (FSRS) technique allows time-gating of the excited-state Raman measurement relative to the initial actinic excitation.[37,38] Although traditionally used to follow the dynamics of a molecule propagating along the S_1 potential energy surface, we recently demonstrated that mode-specific resonance enhancement of the FSRS signal probes the topology of the higher-lying potential energy surfaces.[35,36] Our proof-of-principle measurement for the non-reactive model compound diphenylthiophene (DPT) shows good agreement between the experimental mode-specific resonance enhancements and the calculated gradients of the higher-lying states from high-level calculations, demonstrating the ability of FSRS to probe the topology of higher-lying excited-state potential energy surfaces.[35]

In this contribution, we use resonance-enhanced FSRS to gain new insight into the ultrafast dynamics on the upper-state potential energy surfaces of DAE. The FSRS scheme parallels the sequential two-photon excitation experiments by probing the dynamics of higher-lying excited states that are accessible from S_1. The wavelength dependence of the secondary excitation in the sequential two-photon process sets the stage for studying state-dependent dynamics on the upper-state potential energy surfaces based on resonance-enhanced FSRS measurements. Specifically, we measure the excited-state Raman spectrum of DAEc at two different Raman pump wavelengths—400 and 750 nm—corresponding to different transitions in the excited-state absorption spectrum. The mode-specific enhancements reveal differences in the initial dynamics immediately following secondary excitation. We discuss the results in the context of the earlier pump–repump–probe measurements showing time- and wavelength-dependent enhancement of the cycloreversion yield for sequential excitation.

II. EXPERIMENTAL METHODS

We measure the ground- and excited-state Raman spectra of 1,2-bis(2,4-dimethyl-5-phenyl-3-thienyl)-perfluorocyclopentene (DAE, Fig. 1) using the femtosecond stimulated Raman scattering technique.[39–46] The samples consist of 5 or 10 mM solutions of DAE in cyclohexane (spectroscopic grade, Fisher Scientific). We obtain DAE from TCI America in the transparent, open-ring form (DAEo) and use it without further purification. Irradiating the sample solution with a 310 nm LED for several hours converts the compound to a photostationary state consisting of primarily the closed-ring isomer (DAEc). Only DAEc contributes to the ground- and excited-state Raman spectra that we measure, due to the lower concentration and the weaker overall Raman activity of the open-ring isomer.[15,47] We use a gear pump to flow the sample solution through an optical

cell with 1 mm thick CaF_2 windows and 0.5 mm path length. The 310 nm LED continuously irradiates the sample reservoir during the measurements, to maintain the photostationary state of the recirculating ~20 ml solution over several hours of laser excitation. Optical absorption spectra measured before and after the experiment show no evidence of photodamage.

The FSRS measurements use the output of an amplified Ti:sapphire laser (Coherent, Legend Elite HP) that produces 35 fs pulses at 1 kHz repetition rate. The laser fundamental is split into three separate beams to generate the actinic pump, Raman pump, and white-light probe pulses. First, a commercial optical parametric amplifier (OPA) with two additional stages of non-linear frequency conversion converts one portion of the laser output to 560 nm actinic pump pulses (50 fs and 7.0 μJ at the sample). Next, we use either the output from a second OPA or a second portion of the laser fundamental to obtain narrowband Raman pump pulses via second harmonic generation and spectral filtering. Passing the frequency-doubled light at either 750 or 400 nm through a $4f$ spatial filter gives 1.0 μJ pulses of 1–2 ps duration and ~15 cm^{-1} bandwidth.[46,48] Finally, we obtain broadband fs probe pulses by focusing a small portion of the laser fundamental into a continuously translating CaF_2 window mounted on a circular translation stage for white-light continuum generation. All three resulting laser beams have vertical polarization and propagate in the plane of the laser table before intersecting in the sample at a small angle. Synchronized optical choppers block the actinic pump at 500 Hz and the Raman pump at 250 Hz for active background subtraction.

After the sample, a 1/4 m imaging spectrograph (Newport, MS260i) disperses the probe light onto a 2068 pixel linear CCD array (Hamamatsu, S11156-2048) for shot-to-shot detection. We use an entry slit of 50 μm and either a 1200 or 2400 line/mm grating (for the measurements using 750 and 400 nm Raman pump wavelength, respectively), to achieve an ~10 cm^{-1} resolution. A neutral density filter attenuates the probe light after the sample in order to match the dynamic range of the CCD array detector. The ground-state stimulated Raman signal is obtained from the ratio of the probe intensity with and without the Raman pump incident on the sample, both with the actinic beam blocked. The excited-state Raman spectrum is calculated as the difference between the Raman gain obtained with and without the actinic pump. We typically average over 4 $\times 10^6$ combinations of the actinic and Raman pump pulse sequences (16×10^6 laser shots) per spectrum. The baseline correction methods are described in the supplementary material.

For comparison with the experimental results, we also calculate the ground- and excited-state Raman spectra of DAEc. We calculate the ground-state spectrum using density functional theory (DFT) with B3LYP/aug-cc-pVDZ, and the excited-state spectrum using time-dependent DFT (TD-DFT) with B3LYP/6-31+G*. In each case, we find the optimized geometry and normal mode coordinates and then obtain the Raman intensities by numerical differentiation of the polarizability tensor in each normal mode coordinate using analytical polarizabilities.[34] The calculations use a development version of GAUSSIAN.[49] No resonance condition is explicitly included in either the ground- or excited-state calculations. However, we note that resonance enhancement only affects the magnitude of the Raman scattering and not the frequencies.[50] Previous work shows good agreement between the experimental and calculated frequencies at these levels of theory,[51] even in the excited state.[34–36,52]

III. RESULTS AND ANALYSIS

A. Transient absorption and ground-state Raman spectroscopy

The excited-state dynamics of DAEc have been reported previously, including both TA and FSRS measurements.[15,16,22,53–55] In order to provide a reference for the excited-state Raman measurements that we present below, Fig. 2 shows the evolution of the TA spectrum following actinic excitation at 560 nm. The transient spectrum includes overlapping contributions from both ground-state bleaching (centered near 550 nm) and excited-state absorption. The excited-state lifetime of ~9 ps and cycloreversion yield of only ~0.02 result in complete decay of the excited-state absorption bands and significant recovery of the ground-state bleach within tens of ps, after which the signal no longer changes.[13,15,23] Importantly, anisotropy measurements (see the supplementary material) indicate that the excited-state absorption probes different transitions in the 400–450 nm and 650–750 nm ranges.[56] The wavelength-dependence of the sequential two-photon excitation experiments described in the introduction section also points to different transitions in these two regions of the excited-state spectrum.[23] These are the two regions that we probe in the FSRS spectra presented below.

The ground-state Raman spectrum of DAEc provides another important reference point for comparison with the excited-state measurements. Figure 3 shows the stimulated Raman spectrum that we obtain with the 750 nm Raman excitation, as well as the calculated spectrum and the spectrum of neat cyclohexane, the latter of which has been subtracted from the experimental spectra throughout this paper. The stimulated Raman spectrum of DAEc closely resembles the spontaneous Raman spectrum that we obtain using a commercial spectrometer at 785 nm, except for a few transitions

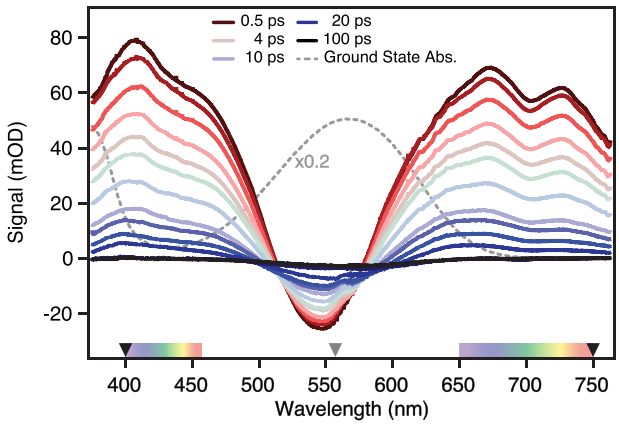

FIG. 2. Evolution of the optical TA spectrum of DAEc following actinic excitation at 560 nm. The gray dashed line shows the ground-state absorption for comparison. The gray marker indicates the actinic excitation wavelength, and black markers and color bars indicate the Raman pump and probe wavelengths, respectively.

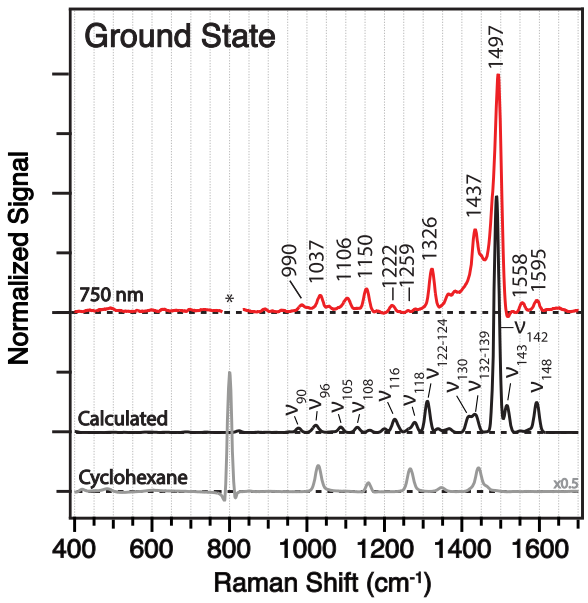

FIG. 3. Ground-state Raman spectrum of DAEc. The experimental spectrum (red) is from stimulated Raman scattering at 750 nm excitation with an anti-Stokes probe. The calculated spectrum (black) includes a 0.970 frequency scaling factor and a 15 cm^{-1} broadening. The Raman spectrum of the neat solvent is also shown for comparison.

with slightly higher intensity due to resonance enhancement effects.[57] Notably, the stimulated Raman measurements at 750 nm use an anti-Stokes probe light that partially overlaps the tail of the ground-state absorption band of DAEc (see Fig. 2). The observed frequencies for several of the most intense Raman bands in the ground-state spectrum of DAEc are listed in Table I, along with the calculated transition frequencies and vibrational mode assignments. A complete table of calculated frequencies and intensities is available in the supplementary material.

We assign the experimental bands in the ground-state spectrum by comparison with the calculations. For example, we assign the dominant vibrational band at 1497 cm^{-1} as a delocalized ethylenic stretching mode that extends along the backbone of the molecule (ν_{142} in the calculations). Some of the experimental bands have contributions from several closely spaced transitions, such as the band near 1437 cm^{-1} (ν_{132}–ν_{139}), but in most cases we identify a single transition that is most likely responsible for the observed band.[34,52] Subtle differences in the relative intensities of the experimental and calculated spectra also reveal mode-specific resonance enhancement effects for some of the stimulated Raman bands. For example, the band at 1558 cm^{-1} is relatively strong in the experimental spectrum, compared to the calculated spectrum, which does not include any resonance enhancement effects. The assignment of this band as a delocalized backbone stretching mode (ν_{144}) is relatively straightforward, based on the consideration of the resonance condition for $\pi\pi^*$ excitation and the relatively low density of vibrational states in this region of the spectrum. A more detailed analysis of the

TABLE I. Assignment of ground-state Raman bands.

Expt. (cm^{-1})	Calc.[a] (cm^{-1})	Mode	Mode assignment[b]
990	978	$\nu_{89/90}$	Phenyl ring breathing
1037	1022	$\nu_{96/97}$	Phenyl CH wag
1106	1087	ν_{105}	CHD ring breathing, methyl str.
1150	1129	ν_{108}	C–C str. in CHD ring and methyl
⋯	1152	ν_{111}	C–C str. localized in CHD ring, methyl bend
1222	1199	ν_{114}	C–C str. in CHD ring
⋯	1225	ν_{116}	Delocalized backbone str.
1259	1234	ν_{117}	Delocalized backbone str., inter-ring C–C str.
⋯	1262	ν_{118}	C–C str of central rings
⋯	1277	ν_{119}	C–C str. in phenyl, CH wag
⋯	1309	$\nu_{122/123}$	CH wag in phenyl, low amp backbone str.
1326	1312	ν_{124}	Delocalized backbone stretching
⋯	1415	$\nu_{130/131}$	Localized C–C phenyl str. and CH wag
1437	1424–39	$\nu_{132–139}$	Methyl CH bend and umbrella (mixed)
1497	1490	ν_{142}	C=C backbone str., methyl umbrella
⋯	1515	ν_{143}	C=C backbone str., phenyl CH wag
1558	1550	ν_{144}	Deloc. C=C backbone str.; higher amp. in CHD
⋯	1564	ν_{145}	Localized C–C phenyl ring str.
⋯	1574	ν_{147}	C=C str. in CHD
1595	1592	$\nu_{148/149}$	Localized C–C phenyl ring str.

[a]B3LYP/aug-cc-pVDZ with 0.970 frequency scaling factor.
[b]CHD = Cyclohexadiene.

ground-state resonance Raman spectrum of DAEc was presented elsewhere.[57]

B. Excited-state resonance Raman spectroscopy

Turning to the excited state, Fig. 4 shows the resonance-enhanced FSRS spectra that we obtain using Raman excitation wavelengths of 750 and 400 nm. For each Raman excitation wavelength, we report spectra for time delays of 0.3 and 5.0 ps after the actinic excitation at 560 nm. The excited-state measurements are complicated by attenuation of the Raman pump and probe pulses, due to transient absorption by the excited molecules. Resonant excitation by the Raman pump pulses results in both bleaching of the excited-state absorption bands and reduced ground-state and solvent scattering signals, due to depletion of the Raman pump pulses. Together, these effects complicate the signal processing, but have been compensated by suitable background subtraction and baseline correction methods, as described in the supplementary material. The resulting spectrum for the 750 nm Raman excitation at 0.3 ps is in very good agreement with the FSRS spectrum of DAEc measured with an 800 nm Raman excitation and a Stokes probe light by Valley *et al.*[53] We are not aware of previous FSRS measurements for DAEc at any other Raman excitation wavelengths.

Notable transitions in the 750 nm FSRS spectrum at 0.3 ps include the bands at 1580, 1508, 1343, 1308, 1188, and 1001 cm^{-1}. There are many additional bands with lower intensity, especially in the lower-frequency region of the spectrum below 800 cm^{-1}. Several of the same transitions are also evident in the 400 nm FSRS spectrum, including bands near 1587, 1503, and 1188 cm^{-1}, to which we assign the same vibrations as in the 750 nm spectrum, despite the slightly different frequencies for the two higher-frequency bands. In other regions of the spectrum, there are more significant differences in intensity between the Raman excitation wavelengths. For example, some transitions are relatively strong in the 400 nm spectrum compared to the 750 nm spectrum (e.g., 1263 and 1443 cm^{-1} bands), whereas others are much weaker (1188 cm^{-1}) or missing from the 400 nm spectrum altogether (1308 and 1343 cm^{-1}). We also note that the intense and well-defined 1001 cm^{-1} band in the 750 nm spectrum is replaced by a pair of transitions at 987 and 1026 cm^{-1} in the 400 nm spectrum.

The time dependence of the FSRS spectrum is similar at 400 and 750 nm, with the overall Raman signal strength falling by about half at most frequencies due to the declining excited-state population. An exception is the 1503/1508 cm^{-1} band, which decays almost entirely to the baseline on this timescale, regardless of the excitation wavelength. We also observe a very broad band (or collection of bands) in the 1420–1480 cm^{-1} range of the 750 nm spectrum at 5 ps. The broad feature may be related to incomplete subtraction of the ground-state spectrum, which has a broad baseline in this frequency range, or it could reflect a contribution from vibrationally hot molecules that return to the ground state on this timescale. The broad feature is absent from the 400 nm spectrum at 5 ps, possibly because that excitation wavelength is less sensitive to resonance enhancement for vibrationally hot molecules in the ground electronic state. The band is also absent from the spectrum reported by Valley *et al.*,[53] possibly due to that measurement (800 nm pump, Stokes probe) being farther from the resonance with the ground-state absorption. We are currently examining the time-evolution in more detail in order to better understand the origin of this transient Raman band.

Figure 4 shows the calculated excited-state Raman spectrum of DAEc for comparison with the experimental FSRS spectra. Importantly, the calculated spectrum, which is the same in both

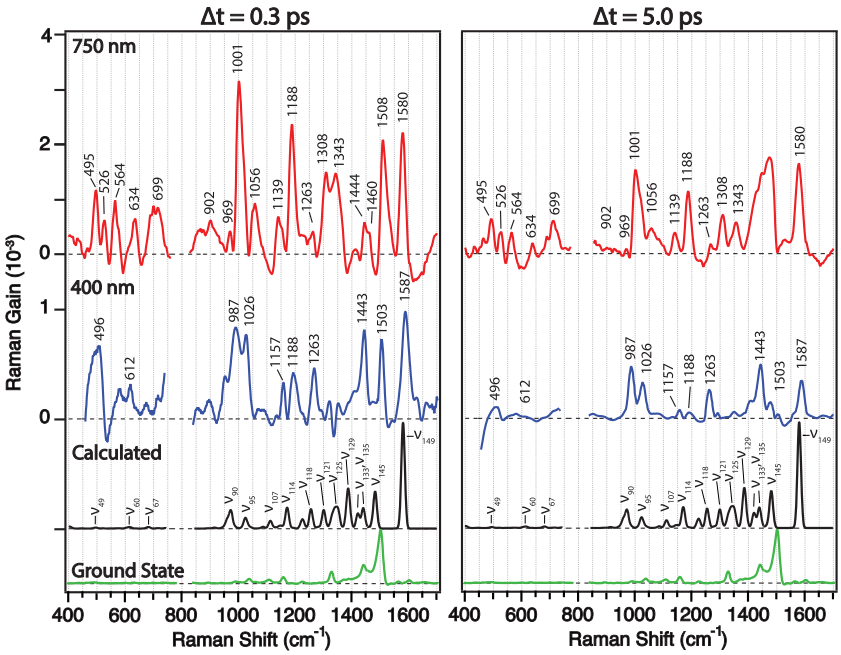

FIG. 4. Excited-state resonance Raman spectra following actinic excitation of DAEc at 560 nm. The left panel shows experimental FSRS spectra at a time delay of 0.3 ps; the right panel shows the spectra at 5 ps delay. From top to bottom, each panel shows the experimental FSRS spectra at 750 nm (red) and 400 nm (blue), the calculated spectrum (black), and the experimental ground-state spectrum (green). The calculated spectrum includes a 0.963 frequency scaling factor and a 15 cm^{-1} broadening, but neglects resonance-enhancement effects. All FSRS spectra have been corrected for ground state bleach.

panels of the figure, does not include any resonance-enhancement effects, whereas both experimental FSRS spectra are in resonance with excited-state absorption bands. The calculated Raman spectrum also depends on the optimized geometry of the excited state. Optimization of the first excited state results in a local minimum that is located relatively close to the Franck–Condon (FC) point. The main structural differences at the local minimum compared to the FC geometry include reduced bond alternation along the conjugated backbone, elongation of the reactive C–C bond (from 1.542 to 1.592 Å), and slight planarization of the phenyl rings relative to the thiophene rings. The local minimum is 1680 cm^{-1} below the FC point of S_1 at the B3LYP/6-31+G* level of theory.

The calculated spectrum at this single point provides a static snapshot that is independent of any dynamics on the S_1 potential energy surface. Although the frequencies and intensities depend on the precise structure of the molecule, the calculations represent a useful point of comparison that is independent of the electronic resonance condition. Table II lists the mode assignments for many of the experimental Raman bands, based on comparison with the calculations. A complete list of the calculated transition frequencies and intensities for the excited state is available in the supplementary material. The calculated intensities tend to decrease with decreasing frequency, reminiscent of the ground-state spectrum,[58] but in stark contrast with the experimental resonance Raman spectra at both 750 and 400 nm. We previously observed a similar preference for resonance enhancement of the low-frequency modes in the excited-state Raman spectra of several aryl-substituted thienyl compounds.[34–36]

TABLE II. Excited-state Raman band assignments.

750 nm (cm^{-1})	400 nm (cm^{-1})	Calc.[a] (cm^{-1})	Mode[b]	Description[c]
...	...	490	ν_{48}	CHD and thiophene ring breathing, phenyl deformation
495	496	496	ν_{49}	C–S str., out of plane CH wag on phenyl
526	...	519	ν_{51}	C–S str., CHD and phenyl ring deformation
...	...	550	ν_{53}	Out of plane ring torsion of thiophene and CHD
564	...	566	ν_{55}	Out of plane torsion of phenyl, CHD ring breathing, CH rock
...	579	580	ν_{56}	Out of plane backbone deformation
...	612	615	ν_{60}	Out of plane torsion of backbone, phenyl ring breathing
634	...	638	ν_{62}	C–S str. and CHD ring torsion
699	...	682	$\nu_{66/67}$	Phenyl CH out of plane rock
902	...	915	ν_{81}	C–S str. and phenyl ring breathing
...	...	959	ν_{86}	Delocalized ring breathing of CHD, thio and phenyl
969	...	973	ν_{90}	Phenyl ring deformation
...	987	987	ν_{91}	Phenyl ring breathing, C=C str. in thiophene, CH wag
1001	...	1005	ν_{92}	CHD and cyclopentane ring deformation, methyl C–C str.
...	...	1023	ν_{95}	Methyl and phenyl CH wag
...	1026	1027	ν_{98}	Methyl CH wag
1056	...	1060	ν_{102}	CHD C–C str., methyl CH rock
...	...	1112	$\nu_{106/107}$	C–C str. in CHD, cyclopentane breathing and CH wag
1139	...	1142	ν_{109}	C–C str. in CHD ring and umbrella motions of methyl
...	1157	1152	ν_{112}	C–C str. between CHD and thiophene rings
...	...	1172	$\nu_{113/114}$	CH rock in phenyl rings
1188	1188	1191	ν_{115}	C–C str. in CHD ring, phenyl and cyclopentane, methyl umbrella
...	...	1228	$\nu_{116/117}$	C–C str. between phenyl and thiophene, phenyl CH rock
1263	1263	1255	ν_{118}	Delocalized backbone str., cyclopentane C–C str.
1308	...	1300	ν_{121}	C–C str. of CHD, thio and cyclopentane, CH rock
...	...	1330	ν_{124}	C–C str. in central ring, phenyl CH rock
1343	...	1340	ν_{125}	C=C str. in central rings and cyclopentane
...	...	1351	ν_{126}	C–C str. in central rings, methyl umbrella
...	...	1386	ν_{129}	Backbone C=C str., methyl umbrella
...	...	1392	$\nu_{130/131}$	Methyl umbrella, C=C str. in thiophene
...	...	1421	ν_{133}	C–C str of carbon backbone, phenyl CH rock
1444	1443	1440	$\nu_{134/135}$	C=C str. along carbon backbone, methyl umbrella
1508	1503	1482	$\nu_{144/145}$	C=C str. along carbon backbone, CH rock
1580	1587	1581	$\nu_{148/149}$	Localized C–C str. in phenyl rings

[a]B3LYP/6-31+G* with 0.963 frequency scaling factor.
[b]Degenerate or nearly degenerate modes indicated as $\nu_{n/m}$.
[c]CHD refers to the central cyclohexadiene ring.

We tentatively assign the highest-frequency band in each of the experimental FSRS spectra as a pair of nearly degenerate modes $\nu_{148/149}$ that are responsible for the strongest transition in the calculated spectrum. The slightly different frequencies for these two experimental bands, 1580 and 1587 cm^{-1}, may reflect background subtraction error in this region of the spectrum. Nevertheless, the assignment of this mode is relatively straightforward, because it is well isolated from the other transitions and is one of the most intense bands in both experimental and calculated spectra. Interestingly, this transition excites a localized phenyl ring stretching mode, rather than the delocalized C=C stretching mode that dominates the ground-state spectrum (ν_{142} at 1497 cm^{-1}). In the excited state, we assign the experimental bands at 1508/1503 and 1443 cm^{-1} as nearly degenerate pairs of backbone stretching modes $\nu_{144/145}$ and $\nu_{134/135}$, respectively, with the latter having more intensity in the 400 nm spectrum due to mode-specific resonance enhancement at that excitation wavelength. The different intensities and the large frequency shift for the delocalized C=C stretching modes between the ground and excited states reflect differences in conjugation between the two electronic states due to the different π electron densities.

The excited-state Raman spectrum becomes more congested at lower frequencies. Figure 5 shows an expanded view of the 1000–1400 cm^{-1} range of the spectrum, including sticks that represent the calculated transition intensities. The stick spectrum illustrates the relatively high density of vibrational states in this region, and mode assignments are further complicated by the resonance condition, which has a significant impact on the observed intensities compared to the off-resonance calculations.[34] For example, the bands at 1343 and 1308 cm^{-1} in the 750 nm spectrum are barely distinguishable from the noise in the 400 nm spectrum. We assign these bands as ν_{125} and ν_{121}, respectively, both of which involve stretching in the central region of the molecule, including the cyclohexadiene ring. In contrast, the band near 1263 cm^{-1} in the 400 nm spectrum, which we assign as a delocalized backbone stretching mode, ν_{118}, is very weak in the 750 nm spectrum. These mode-specific resonance enhancements illustrate differences in the upper electronic states that are accessed by excitation at the two wavelengths.

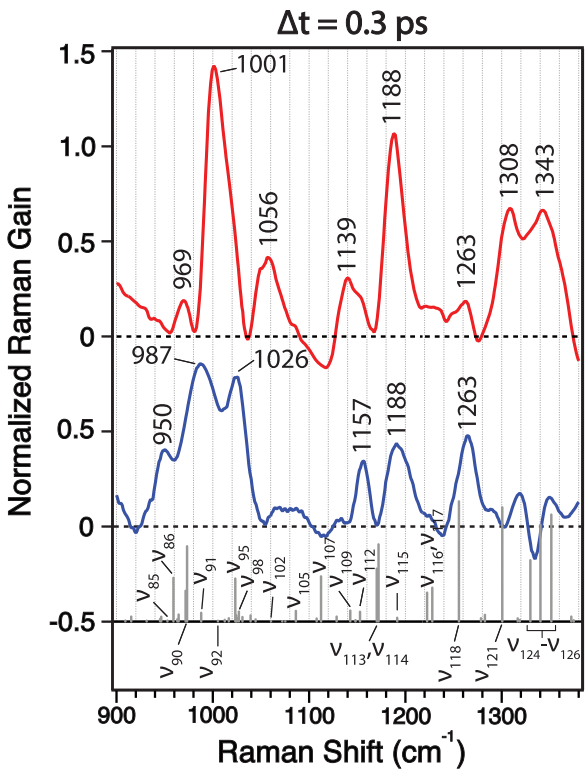

FIG. 5. Excited-state resonance Raman spectra in the 900–1400 cm^{-1} region for the 750 and 400 nm excitation (red and blue, respectively). Sticks represent the calculated Raman transitions after applying the frequency correction of 0.963. The calculations do not account for resonance enhancement effects.

Other assignments in the 1000–1400 cm^{-1} region of the Raman spectrum include the bands near 1188, 1139, 1056, and 1001 cm^{-1} in the 750 nm spectrum, and at 1188, 1157, 1026, and 987 cm^{-1} in the 400 nm spectrum. The band near 1188 cm^{-1}, which appears in both experimental spectra, but has very little intensity in the calculated spectrum, is assigned as ν_{115}, a C–C stretching mode that includes significant displacement of the reactive C–C bond in the cyclohexadiene ring. The assignment of ν_{115} is based on a relatively large frequency gap compared to the adjacent vibrations, and the consideration that this motion is more likely to gain intensity from resonance with π-conjugated excitation than the nearby C–H rocking mode. This band was previously identified by Valley *et al.*[53] as a key C–C stretching mode related to the cycloreversion reaction coordinate. In fact, we find that many of the modes that have the most significant resonance enhancement in the 750 nm spectrum involve vibrations with significant displacements in the central region of the molecule, including the cyclohexadiene ring that undergoes cycloreversion, in contrast with the more delocalized modes that are enhanced in the 400 nm spectrum.

IV. DISCUSSION

Mode-specific resonance enhancements in the excited-state resonance Raman spectra measured at 750 and 400 nm reveal new information about the initial dynamics following secondary excitation from S_1 to the higher-lying excited states of DAEc. Previous experiments examined the mechanism for sequential excitation using time-resolved pump–repump–probe spectroscopy (PReP).[22,23] The PReP measurements show that re-excitation at 400 nm increases the quantum yield only after a delay of several ps, suggesting that the secondary excitation does not access a more reactive region of the upper-state potential energy surface until after the molecule overcomes a barrier on the S_1 surface (Fig. 6). In contrast, re-excitation at 750 nm results in increased cycloreversion for delays as short as 100 fs after the initial excitation, suggesting that secondary excitation at this wavelength accesses a more reactive region of the upper state almost immediately.[23]

The FSRS measurement mirrors the PReP experiment by probing the higher-lying states of DAEc at various points along the S_1 reaction coordinate. Thus, the time-dependent FSRS spectra in Fig. 4 provide a complementary way to probe the mechanism for sequential two-photon excitation. For example, differences in

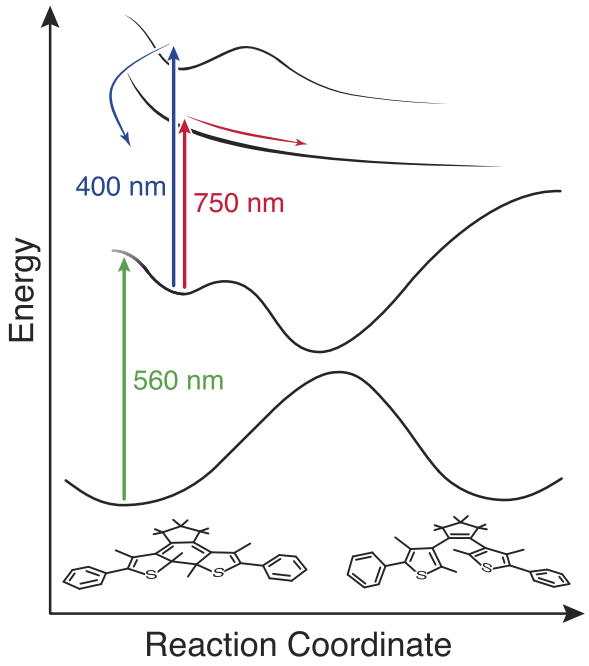

FIG. 6. Schematic diagram of the reaction dynamics upon sequential excitation at 750 and 400 nm. Adapted from Ref. 23.

the mode-specific enhancements at 750 and 400 nm illustrate the different initial wave packet motions for re-excitation at these wavelengths. According to the Woodward–Hoffman rules,[59] the cycloreversion reaction involves conrotatory motion in the central cyclohexadiene ring that ultimately breaks the C–C σ-bond and provides a pathway to the open-ring isomer. Therefore, we anticipate that vibrations preserving the C_2 symmetry of the molecule will promote the cycloreversion reaction. Valley *et al.*,[53] identified excited-state Raman bands at 1181 and 1333 cm^{-1} as vibrations localized on the cyclohexadiene ring that represent motion along this ring-opening reaction coordinate. They also observed a band at 993 cm^{-1}, which they assigned as a phenyl ring bending mode that is orthogonal to the reaction coordinate. Molecular dynamics simulations by Chiariello *et al.*,[60] support these interpretations by showing that the 1181 and 1333 cm^{-1} modes play an integral role in the ring-opening reaction.

Beyond simply identifying vibrational modes that map onto the reaction coordinate, excited-state resonance Raman spectroscopy probes the Franck–Condon activity of each mode upon re-excitation to the higher-lying states, S_n, based on the wavelength-dependent intensities. For example, we observe significant enhancement of the Raman bands near 1188 and 1343 cm^{-1} in the 750 nm spectrum. Similar to Valley *et al.*,[53] we assign these bands as vibrations involving C–C stretching of the cyclohexadiene ring, which suggests that re-excitation at this wavelength launches a wave packet on the upper state that initially moves along the cycloreversion reaction coordinate (Fig. 6). In addition, we observe mode-specific enhancement of the bands near 1308, 1139, 1056, and 1001 cm^{-1}, which are all identified by comparison with the calculations as having stretching motions related to the cyclohexadiene ring-opening reaction coordinate. These mode-specific enhancements suggest that the initial wave packet motion on the upper state following sequential excitation at 750 nm maps directly onto the cycloreversion reaction coordinate.

In contrast with the enhancements at 750 nm, the 400 nm spectrum reveals resonance enhancement for vibrations that do not directly promote the cycloreversion reaction. For example, the strongly enhanced bands near 1263, 1026, and 987 cm^{-1} are assigned as delocalized backbone stretching, C–H wagging, and phenyl ring breathing modes, respectively. We equate the 987 cm^{-1} band in our 400 nm spectrum with the 993 cm^{-1} band identified by Valley *et al.*,[53] a mode involving vibration of the phenyl rings that is orthogonal to the reaction coordinate. We distinguish this band (ν_{97}) from the one near 1001 cm^{-1} (ν_{92}), which is significantly enhanced in the 750 nm spectrum, and that we assign as cyclohexadiene and cyclopentane ring deformations. The band at 1188 cm^{-1} is observed in the 400 nm spectrum; however it is not as strongly enhanced compared to other modes. While this band is assigned as having significant displacement in the cyclohexadiene ring, it is combined with other resonance-enhanced vibrations in the 400 nm spectrum that compete with the motion along the C–C bond-breaking coordinate, thus diminishing the overall projection of the initial wave packet onto the reaction coordinate for excitation at this wavelength.

Importantly, the different relative intensities in the excited-state resonance Raman spectra at 750 and 400 nm illustrate different initial motions of the wave packet upon re-excitation from S_1 to S_n. Re-excitation at 750 nm initiates a wave packet that has significant motion along the cycloreversion reaction coordinate, consistent with the PReP measurements showing enhanced reaction yield for this re-excitation wavelength at short pump–repump delay times.[23] In contrast, re-excitation at 400 nm initiates a wave packet that initially moves along coordinates that are counterproductive, which explains the lack of enhanced reactivity for secondary re-excitation at short pump–repump delay times (Fig. 6). Indeed, the PReP measurements indicate that the enhanced yield for the 400 nm re-excitation requires a few-ps time delay between the first and second excitation laser pulses in order to increase the reaction yield.[22]

Time-gating of the resonance Raman measurement has the potential to probe the gradients (and, therefore, the initial dynamics) of the upper-state potential energy surfaces at various points along the S_1 reaction path. Although a full analysis of the time-evolution is beyond the scope of this paper, we observe important differences in the FSRS spectra at 0.3 and 5 ps time delays. For example, the 1508/1503 cm^{-1} band decays within 5 ps for both excitation wavelengths, which is much faster than for other vibrations. The rapid decay of this band may reflect a change in the molecular structure associated with changes in the π-conjugation, possibly including C–C bond breaking as the molecule overcomes a barrier on the S_1 surface.[61] Although we anticipated an increase in the relative intensities of vibrations that map onto the reaction coordinate at the longer delay time for 400 nm re-excitation, this is not the case. We also find it somewhat surprising that the frequencies of the vibrational bands do not change very much between 0.3 and 5 ps in either spectrum, although we note that the broad set of vibrational bands near 1420–1480 cm^{-1} in the 750 nm spectrum may probe return to the ground electronic state on a ~9 ps timescale. A more complete

analysis of the time-evolution of the FSRS signals at 750 and 400 nm is underway.

V. CONCLUSIONS

We have reported excited-state resonance Raman spectra for a molecular photoswitch using Raman excitation wavelengths of 750 and 400 nm. The resonance Raman spectra at these wavelengths probe the initial wave packet dynamics on different higher-lying excited states, S_n, at well-defined time delays following the initial actinic excitation of the molecule at 560 nm. The FSRS approach allows us to identify the initial motions of the wave packet upon secondary excitation to each of the upper states based on mode-specific enhancements of the Raman bands. The different excitation wavelengths reveal different dynamics. Re-excitation into the lower-energy state at 750 nm populates vibrational modes that are localized in the central region of the molecule and resemble the ring-opening reaction coordinate. In contrast, re-excitation into the higher-energy state at 400 nm populates vibrations that are not directly related to the cycloreversion reaction, suggesting that the initial wave packet motion is largely concentrated in the backbone and peripheral phenyl ring motions that are orthogonal to the reaction coordinate. This work highlights the ability of FSRS to provide detailed new information about the dynamics on higher-lying excited states that is not available using electronic spectroscopy techniques alone.

SUPPLEMENTARY MATERIAL

See the supplementary material for a description of the baseline correction methods, the optical anisotropy spectrum, a comparison of stimulated and spontaneous ground-state Raman spectra, and tables of the coordinates and calculated Raman spectra for ground- and excited-state DAEs.

ACKNOWLEDGMENTS

The authors wish to thank Marco Caricato and Matthew S. Barclay for many helpful discussions and for providing the calculated excited-state Raman spectrum of DAEc. This work was supported by the National Science Foundation (NSF) through Grant No. CHE-1956387. C.G.E. acknowledges support from the Individual Research and Development (IR/D) program while serving as Program Director at NSF.

AUTHOR DECLARATIONS

Conflict of Interest

The authors have no conflicts to disclose.

Author Contributions

Kristen H. Burns: Data curation (equal); Formal analysis (equal); Investigation (equal); Writing – original draft (lead). **Timothy J. Quincy**: Data curation (supporting); Investigation (supporting); Writing – original draft (supporting). **Christopher G. Elles**: Conceptualization (lead); Formal analysis (equal); Funding acquisition (lead); Project administration (lead).

DATA AVAILABILITY

The data that support the findings of this study are available from the corresponding author upon reasonable request.

REFERENCES

[1]L. Hou, T. Leydecker, X. Zhang, W. Rekab, M. Herder, C. Cendra, S. Hecht, I. McCulloch, A. Salleo, E. Orgiu, and P. Samorì, "Engineering optically switchable transistors with improved performance by controlling interactions of diarylethenes in polymer matrices," J. Am. Chem. Soc. **142**, 11050–11059 (2020).

[2]H. Nie, N. S. Schauser, J. L. Self, T. Tabassum, S. Oh, Z. Geng, S. D. Jones, M. S. Zayas, V. G. Reynolds, M. L. Chabinyc, C. J. Hawker, S. Han, C. M. Bates, R. A. Segalman, and J. Read De Alaniz, "Light-switchable and self-healable polymer electrolytes based on dynamic diarylethene and metal-ion coordination," J. Am. Chem. Soc. **143**, 1562–1569 (2021).

[3]H.-B. Cheng, B. Qiao, H. Li, J. Cao, Y. Luo, K. M. Kotraiah Swamy, J. Zhao, Z. Wang, J. Y. Lee, X.-J. Liang, and J. Yoon, "Protein-activatable diarylethene monomer as a smart trigger of noninvasive control over reversible generation of singlet oxygen: A facile, switchable, theranostic strategy for photodynamic-immunotherapy," J. Am. Chem. Soc. **143**, 2413–2422 (2021).

[4]T. Fukushima, K. Tamaki, A. Isobe, T. Hirose, N. Shimizu, H. Takagi, R. Haruki, S. I. Adachi, M. J. Hollamby, and S. Yagai, "Diarylethene-powered light-induced folding of supramolecular polymers," J. Am. Chem. Soc. **143**, 5845–5854 (2021).

[5]I. Hamdi, G. Buntinx, O. Poizat, A. Perrier, L. Le Bras, S. Delbaere, S. Barrau, M. Louati, M. Takeshita, K. Tokushige, M. Takao, and S. Aloïse, "Excited-state dynamics of dithienylethenes functionalized for self-supramolecular assembly," J. Phys. Chem. A **122**, 3572–3582 (2018).

[6]C. L. Sun, C. Wang, and R. Boulatov, "Applications of photoswitches in the storage of solar energy," ChemPhotoChem **3**, 268–283 (2019).

[7]C. R. Honick, G. M. Peters, J. D. Young, J. D. Tovar, and A. E. Bragg, "Core structure dependence of cycloreversion dynamics in diarylethene analogs," Phys. Chem. Chem. Phys. **22**, 3314–3328 (2020).

[8]M. Irie, T. Fukaminato, K. Matsuda, and S. Kobatake, "Photochromism of diarylethene molecules and crystals: Memories, switches, and actuators," Chem. Rev. **114**, 12174–12277 (2014).

[9]K. Matsuda and M. Irie, "Diarylethene as a photoswitching unit," J. Photochem. Photobiol., C **5**, 169–182 (2004).

[10]M. Irie, "Diarylethenes for memories and switches," Chem. Rev. **100**, 1685–1716 (2000).

[11]S. Nakamura and M. Irie, "Thermally irreversible photochromic systems. A theoretical study," J. Org. Chem. **53**, 6136–6138 (1988).

[12]M. Irie and M. Mohri, "Thermally irreversible photochromic systems. Reversible photocyclization of diarylethene derivatives," J. Org. Chem. **53**, 803–808 (1988).

[13]H. Miyasaka, M. Murakami, T. Okada, Y. Nagata, A. Itaya, S. Kobatake, and M. Irie, "Picosecond and femtosecond laser photolysis studies of a photochronic diarylethene derivative: Multiphoton gated reaction," Chem. Phys. Lett. **371**, 40–48 (2003).

[14]Y. Ishibashi, K. Okuno, C. Ota, T. Umesato, T. Katayama, M. Murakami, S. Kobatake, M. Irie, and H. Miyasaka, "Multiphoton-gated cycloreversion reactions of photochromic diarylethene derivatives with low reaction yields upon one-photon visible excitation," Photochem. Photobiol. Sci. **9**, 172–180 (2010).

[15]H. Sotome, T. Nagasaka, K. Une, S. Morikawa, T. Katayama, S. Kobatake, M. Irie, and H. Miyasaka, "Cycloreversion reaction of a diarylethene derivative at higher excited states attained by two-color, two-photon femtosecond pulsed excitation," J. Am. Chem. Soc. **139**, 17159–17167 (2017).

[16]H. Sotome, K. Une, T. Nagasaka, S. Kobatake, M. Irie, and H. Miyasaka, "A dominant factor of the cycloreversion reactivity of diarylethene derivatives as

revealed by femtosecond time-resolved absorption spectroscopy," J. Chem. Phys. **152**, 034301 (2020).
[17]K. Shinoda, S. Yokojima, T. Fukaminato, and S. Nakamura, "Determining factor of the quantum yield of the cyclization reaction via triplet states for dye-attached diarylethene," J. Phys. Chem. A **125**, 5895–5902 (2021).
[18]B. C. Arruda and R. J. Sension, "Ultrafast polyene dynamics: The ring opening of 1,3-cyclohexadiene derivatives," Phys. Chem. Chem. Phys. **16**, 4439–4455 (2014).
[19]T. E. Wiley, A. Konar, N. A. Miller, K. G. Spears, and R. J. Sension, "Primed for efficient motion: Ultrafast excited state dynamics and optical manipulation of a four stage rotary molecular motor," J. Phys. Chem. A **122**, 7548–7558 (2018).
[20]H. Miyasaka, M. Murakami, A. Itaya, D. Guillaumont, S. Nakamura, and M. Irie, "Multiphoton gated photochromic reaction in a diarylethene derivative," J. Am. Chem. Soc. **123**, 753–754 (2001).
[21]K. Tani, Y. Ishibashi, H. Miyasaka, S. Kobatake, and M. Irie, "Dynamics of cyclization, cycloreversion, and multiphoton-gated reaction of a photochromic diarylethene derivative in crystalline phase," J. Phys. Chem. C **112**, 11150–11157 (2008).
[22]C. L. Ward and C. G. Elles, "Controlling the excited-state reaction dynamics of a photochromic molecular switch with sequential two-photon excitation," J. Phys. Chem. Lett. **3**, 2995–3000 (2012).
[23]C. L. Ward and C. G. Elles, "Cycloreversion dynamics of a photochromic molecular switch via one-photon and sequential two-photon excitation," J. Phys. Chem. A **118**, 10011–10019 (2014).
[24]H. Sotome, T. Nagasaka, K. Une, C. Okui, Y. Ishibashi, K. Kamada, S. Kobatake, M. Irie, and H. Miyasaka, "Efficient cycloreversion reaction of a diarylethene derivative in higher excited states attained by off-resonant simultaneous two-photon absorption," J. Phys. Chem. Lett. **8**, 3272–3276 (2017).
[25]R. P. Brady, C. Zhang, J. R. DeFrancisco, B. J. Barrett, L. Cheng, and A. E. Bragg, "Multiphoton control of 6π photocyclization via state-dependent reactant–product correlations," J. Phys. Chem. Lett. **12**, 9493–9500 (2021).
[26]H. Sotome, H. Okajima, T. Nagasaka, Y. Tachii, A. Sakamoto, S. Kobatake, M. Irie, and H. Miyasaka, "Geometrical evolution and formation of the photoproduct in the cycloreversion reaction of a diarylethene derivative probed by vibrational spectroscopy," ChemPhysChem **21**, 1524–1530 (2020).
[27]T. Nagasaka, H. Sotome, S. Morikawa, L. M. Uriarte, M. Sliwa, T. Kawai, and H. Miyasaka, "Restriction of the conrotatory motion in photo-induced 6π electrocyclic reaction: Formation of the excited state of the closed-ring isomer in the cyclization," RSC Adv. **10**, 20038–20045 (2020).
[28]D. W. McCamant, P. Kukura, and R. A. Mathies, "Femtosecond broadband stimulated Raman: A new approach for high-performance vibrational spectroscopy," Appl. Spectrosc. **57**, 1317–1323 (2003).
[29]S.-Y. Lee and E. J. Heller, "Time-dependent theory of Raman scattering," J. Chem. Phys. **71**, 4777–4788 (1979).
[30]E. J. Heller, R. Sundberg, and D. Tannor, "Simple aspects of Raman scattering," J. Phys. Chem. **86**, 1822–1833 (1982).
[31]A. C. Albrecht, "On the theory of Raman intensities," J. Chem. Phys. **34**, 1476–1484 (1961).
[32]A. B. Myers, R. A. Mathies, D. J. Tannor, and E. J. Heller, "Excited state geometry changes from preresonance Raman intensities: Isoprene and hexatriene," J. Chem. Phys. **77**, 3857–3866 (1982).
[33]G. Batignani, G. Fumero, E. Mai, M. Martinati, and T. Scopigno, "Stimulated Raman lineshapes in the large light–matter interaction limit," Opt. Mater.: X **13**, 100134 (2022).
[34]M. S. Barclay, T. J. Quincy, D. B. Williams-Young, M. Caricato, and C. G. Elles, "Accurate assignments of excited-state resonance Raman spectra: A benchmark study combining experiment and theory," J. Phys. Chem. A **121**, 7937–7946 (2017).
[35]T. J. Quincy, M. S. Barclay, M. Caricato, and C. G. Elles, "Probing dynamics in higher-lying electronic states with resonance-enhanced femtosecond stimulated Raman spectroscopy," J. Phys. Chem. A **122**, 8308–8319 (2018).
[36]M. S. Barclay, M. Caricato, and C. G. Elles, "Femtosecond stimulated Raman scattering from triplet electronic states: Experimental and theoretical study of resonance enhancements," J. Phys. Chem. A **123**, 7720–7732 (2019).
[37]M. Quick, A. L. Dobryakov, S. A. Kovalenko, and N. P. Ernsting, "Resonance femtosecond-stimulated Raman spectroscopy without actinic excitation showing low-frequency vibrational activity in the S_2 state of all-trans β-carotene," J. Phys. Chem. Lett. **6**, 1216–1220 (2015).
[38]W. Yu, J. Zhou, and A. E. Bragg, "Exciton conformational dynamics of poly(3-hexylthiophene) (P3HT) in solution from time-resolved resonant-Raman spectroscopy," J. Phys. Chem. Lett. **3**, 1321–1328 (2012).
[39]D. W. McCamant, P. Kukura, and R. A. Mathies, "Femtosecond time-resolved stimulated Raman spectroscopy: Application to the ultrafast internal conversion in β-carotene," J. Phys. Chem. A **107**, 8208–8214 (2003).
[40]D. W. McCamant, P. Kukura, S. Yoon, and R. A. Mathies, "Femtosecond broadband stimulated Raman spectroscopy: Apparatus and methods," Rev. Sci. Instrum. **75**, 4971–4980 (2004).
[41]S.-Y. Lee, D. Zhang, D. W. McCamant, P. Kukura, and R. A. Mathies, "Theory of femtosecond stimulated Raman spectroscopy," J. Chem. Phys. **121**, 3632–3642 (2004).
[42]P. Kukura, D. W. McCamant, and R. A. Mathies, "Femtosecond stimulated Raman spectroscopy," Annu. Rev. Phys. Chem. **58**, 461–488 (2007).
[43]R. R. Frontiera and R. A. Mathies, "Femtosecond stimulated Raman spectroscopy," Laser Photonics Rev. **5**, 102–113 (2011).
[44]D. R. Dietze and R. A. Mathies, "Femtosecond stimulated Raman spectroscopy," ChemPhysChem **17**, 1224–1251 (2016).
[45]P. Roy, A. S. Sardjan, A. Cnossen, W. R. Browne, B. L. Feringa, and S. R. Meech, "Excited state structure correlates with efficient photoconversion in unidirectional motors," J. Phys. Chem. Lett. **12**, 3367–3372 (2021).
[46]G. Batignani, C. Ferrante, and T. Scopigno, "Accessing excited state molecular vibrations by femtosecond stimulated Raman spectroscopy," J. Phys. Chem. Lett. **11**, 7805–7813 (2020).
[47]E. Pontecorvo, C. Ferrante, C. G. Elles, and T. Scopigno, "Structural rearrangement accompanying the ultrafast electrocyclization reaction of a photochromic molecular switch," J. Phys. Chem. B **118**, 6915–6921 (2014).
[48]E. Pontecorvo, C. Ferrante, C. G. Elles, and T. Scopigno, "Spectrally tailored narrowband pulses for femtosecond stimulated Raman spectroscopy in the range 330–750 nm," Opt. Express **21**, 6866 (2013).
[49]M. J. Frisch, G. W. Trucks, H. B. Schlegel, G. E. Scuseria, M. A. Robb, J. R. Cheeseman, J. A. Montgomery, Jr., T. Vreven, K. N. Kudin, J. C. Burant, J. M. Millam, S. S. Iyengar, J. Tomasi, V. Barone, B. Mennucci, M. Cossi, G. Scalmani, N. Rega, G. A. Petersson, H. Nakatsuji, M. Hada, M. Ehara, K. Toyota, R. Fukuda, J. Hasegawa, M. Ishida, T. Nakajima, Y. Honda, O. Kitao, H. Nakai, M. Klene, X. Li, J. E. Knox, H. P. Hratchian, J. B. Cross, V. Bakken, C. Adamo, J. Jaramillo, R. Gomperts, R. E. Stratmann, O. Yazyev, A. J. Austin, R. Cammi, C. Pomelli, J. W. Ochterski, P. Y. Ayala, K. Morokuma, G. A. Voth, P. Salvador, J. J. Dannenberg, V. G. Zakrzewski, S. Dapprich, A. D. Daniels, M. C. Strain, O. Farkas, D. K. Malick, A. D. Rabuck, K. Raghavachari, J. B. Foresman, J. V. Ortiz, Q. Cui, A. G. Baboul, S. Clifford, J. Cioslowski, B. B. Stefanov, G. Liu, A. Liashenko, P. Piskorz, I. Komaromi, R. L. Martin, D. J. Fox, T. Keith, M. A. Al-Laham, C. Y. Peng, A. Nanayakkara, M. Challacombe, P. M. W. Gill, B. Johnson, W. Chen, M. W. Wong, C. Gonzalez, and J. A. Pople, GAUSSIAN 03, Revision D.01, Gaussian, Inc., 2004.
[50]D. A. Long, *The Raman Effect: A Unified Treatment of the Theory of Raman Scattering by Molecules* (Wiley, New York, 2002), p. 597.
[51]M. S. Barclay, C. G. Elles, and M. Caricato, "Benchmark study of ground-state Raman spectra in conjugated molecules," J. Chem. Theory Comput. **16**, 612–620 (2019).
[52]D. Green, P. Roy, C. R. Hall, J. N. Iuliano, G. A. Jones, A. Lukacs, P. J. Tonge, and S. R. Meech, "Excited state resonance Raman of Flavin mononucleotide: Comparison of theory and experiment," J. Phys. Chem. A **125**, 6171–6179 (2021).
[53]D. T. Valley, D. P. Hoffman, and R. A. Mathies, "Reactive and unreactive pathways in a photochemical ring opening reaction from 2D femtosecond stimulated Raman," Phys. Chem. Chem. Phys. **17**, 9231–9240 (2015).
[54]H. Sotome, D. Kitagawa, T. Nakahama, S. Ito, S. Kobatake, M. Irie, and H. Miyasaka, "Cyclization reaction dynamics of an inverse type diarylethene derivative as revealed by time-resolved absorption and fluorescence spectroscopies," Phys. Chem. Chem. Phys. **21**, 8623–8632 (2019).
[55]A. Jarota, E. Pastorczak, W. Tawfik, B. Xue, R. Kania, H. Abramczyk, and T. Kobayashi, "Exploring the ultrafast dynamics of a diarylethene derivative using sub-10 fs laser pulses," Phys. Chem. Chem. Phys. **21**, 192–204 (2019).

[56]C. L. Ward, "Controlling the cycloreversion reaction of a diarylethene derivative using sequential two-photon excitation," Ph.D. thesis, University of Kansas, 2014.
[57]K. H. Burns and C. G. Elles, "Ultrafast dynamics of a molecular switch from resonance Raman spectroscopy: Comparing visible and UV excitation," J. Phys. Chem. A **126**, 5932–5939 (2022).
[58]M. S. Barclay, C. G. Elles, and M. Caricato, "On the discrepancy between experimental and calculated Raman intensities for conjugated phenyl and thiophene derivatives," J. Phys. Chem. A **124**, 4678–4689 (2020).
[59]R. B. Woodward and R. Hoffmann, "The conservation of orbital symmetry," Angew. Chem., Int. Ed. Engl. **8**, 781–853 (1969).
[60]M. G. Chiariello, U. Raucci, F. Coppola, and N. Rega, "Unveiling anharmonic coupling by means of excited state *ab initio* dynamics: Application to diarylethene photoreactivity," Phys. Chem. Chem. Phys. **21**, 3606–3614 (2019).
[61]M. Boggio-Pasqua, M. Ravaglia, M. J. Bearpark, M. Garavelli, and M. A. Robb, "Can diarylethene photochromism be explained by a reaction path alone? A CASSCF study with model MMVB dynamics," J. Phys. Chem. A **107**, 11139–11152 (2003).